JOM, Vol. 72, No. 9, 2020
https://doi.org/10.1007/s11837-020-04256-8

Tracking Evaporation During Levitation Processing of Nickel-Based Superalloys on the ISS

JANNATUN NAWER,[1] STÉPHANE GOSSÉ,[2] and DOUGLAS M. MATSON[1,3,4]

1.—Mechanical Engineering Department, Tufts University, Medford, MA 02155, USA. 2.—DEN-Service de la Corrosion et du Comportement des Matériaux dans leur Environnement (SCCME), CEA, Université Paris-Saclay, 91191 Gif-sur-Yvette, France. 3.—e-mail: matson@tufts.edu. 4.—e-mail: Douglas.Matson@tufts.edu

Conducting experiments in an inert shielding-gas environment limits the likelihood for experiencing significant mass loss or compositional shifts due to differential relative evaporation. Species-specific evaporation is proven to be below prescribed limits and near-real time monitoring of the potential for exposure is shown to be an effective tool to ensure astronaut safety. The activity coefficients for key constituents in the alloy are defined as a function of temperature for inclusion in next-generation toxicity tracking software.

INTRODUCTION

In order to improve the fidelity of models used for control of the manufacturing processes during fabrication of single-crystal aerospace turbine blades, a series of alloys was selected for investigation by a large collaborative international team using the ESA electromagnetic levitation facility located on board the International Space Station (ISS-EML). A significant portion of this work was aimed at measuring key thermophysical properties including density, viscosity, surface tension, electrical resistivity, and specific heat capacity. When conducting containerless levitation measurement of molten superalloy thermophysical properties, both on ground and in space, monitoring of sample evaporation becomes a concern. Three issues arise. First, change in sample mass over time impacts measurement accuracy. For example, if one is measuring density the experimental procedure involves measuring volume as a function of temperature given the initial mass; if mass were to change one would get erroneous values for apparent density—and the expected deviation will increase with time. Second, for these complex multi-component industrial alloys, changes in sample composition could occur if the alloy experiences differential loss of specific volatile components; you would have the potential to be obtaining the properties of a material which varies over time from the desired target composition. It is thus important to dynamically track evaporation throughout the experiment to ensure that measurement results are both accurate and relevant. Third, and most importantly, astronaut health and safety must be ensured in the event of facility malfunction and it is imperative that evaporation products be held below exposure thresholds.

Tracking is accomplished by breaking the test into discrete time intervals set by the data acquisition. Since the temperature is known at any given interval from the facility pyrometer, the mass loss during that interval can be evaluated and summed to obtain the contribution for all time intervals within a given thermal cycle. This technique requires knowledge of the individual species mass flux as a function of temperature, the system back-pressure used to limit evaporation, and the sample area.

Two approaches have historically been applied for space-based testing. Pre-mission, astronaut safety and health mandates are imposed to mitigate the potential impact from dust emission in the event of catastrophic failure, such as fracture of the facility viewing port. The worst-case scenario would be if all evaporation products were to form dust which could be released into the station's habitable module volume. To reduce potential toxic exposure hazards, engineers at the Microgravity User Support Center (MUSC) use a tool called the Tox-tracker to estimate the evaporative mass loss from the sample after each thermal cycle. Contributions from each cycle are summed for all elemental constituents in the

 (Published online July 8, 2020)

sample and testing is only allowed to continue while all species are below critical threshold limit value (TLV) exposure projections. When any threshold is reached, the facility is shut down for purge/flush cleaning before further processing is allowed.[1]

This pragmatic approach relies on pre-flight evaporative flux measurement. Ground-based evaporation experiments are conducted as a function of melt superheat in vacuum. Tracking of individual elemental constituents assumes ideal solution behavior and loss is apportioned to each component based on initial alloy composition. In orbit, the sample is processed in a chamber that is back-filled with inert gas to reduce evaporation, and since losses are extremely small the sample is assumed to be area and composition invariant over the time frame of interest. This is thus a near real-time empirical technique. During the mission, it is impossible to validate predictions as the sample remains in orbit and is unavailable for spot-checking of the mass until it has been returned to earth.

The second approach relies on use of theoretical predictions based on the Langmuir's equation[2] where m is the mass loss due to evaporation of component i in an n-component system,

$$m_i = \sum_{0}^{t} \sum_{i=1}^{n} \frac{(P_{v,i} - P_{\text{ref}})\alpha_i A_i}{\sqrt{(2\pi M_i \text{RT})}} \Delta t \qquad (1)$$

P_{ref} is the reference pressure, α is the shielding factor, M is the molecular weight, and R is the universal gas constant. Changes in the surface area A are dynamically monitored such that the influence of cumulative mass loss can be aggregated over time and sample dilation with temperature is included with knowledge of alloy thermal expansion coefficient and density. P_{v} is the element-specific vapor pressure which is a function of the reference temperature T during the time increment Δt; it may be calculated using a four-termed expression based on experimental measurements cataloged by Alcock[3] and displayed for the key superalloy constituents in Fig. 1a.

The partial pressure for each alloying element can be calculated by using Raoult's law for an ideal solution where the activity of a component $a_i = \gamma_i c_i$ is assumed to be equal to the concentration c_i of that component in solution; for the ideal case the activity coefficient for each species would be assumed to be $\gamma_i = 1$. The limitations of this approach were demonstrated by Nawer[4] during vacuum levitation experiments using electrostatic levitation (ESL) for the CMSX-10 alloy. The ideal solution model was shown to be a promising approach for most constituents, as confirmed by post-test elemental analysis to verify predicted composition shifts, but significant deviation was observed for aluminum. In this instance, setting the activity coefficient for Al to zero improved the predictive capability of the model to be within $\pm$ 6% error, consistent with observed post-test measurement precision.

Since the activity coefficient accounts for the interactions in the liquid phase between the different constituents in a non-ideal solution, with knowledge of the activity coefficient as a function of temperature the vapor pressure may be evaluated.

$$P_{v,i} = \gamma_i c_i P_v \qquad (2)$$

Lee[5] successfully used the computational thermodynamics program Thermo-Calc to predict activities for iron and cobalt in the equimolar Fe-Co binary mixture to a relative error of 4.8% but to date no complex commercial superalloy has been modeled successfully.

Inert-gas shielding can be accommodated using the empirical correction factor α. This factor is defined as the ratio of the mass losses $v/v_0 = \alpha$ where v represents the loss when gas shielding is employed and v_0 is the corresponding loss in vacuum. Fromm [6] conducted evaporation studies in argon and proposed an empirical relationship

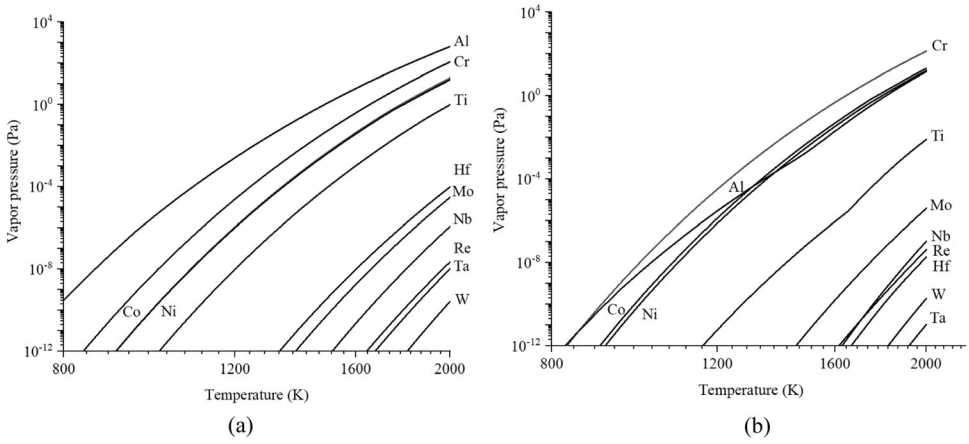

Fig. 1. (a) Pure element and (b) activity-modified vapor pressures of CMSX-10 elements

which attributed shielding to diffusion-limited mass transfer through a gaseous boundary layer at an absolute pressure P such that:

$$\frac{v}{v_0} = \frac{1}{1 + Kp^n} \quad (3)$$

The two empirical constants K and n in Eq. 3 represent fit parameters based on experimental data specific to a given elemental species. For Ni and Co, the recommended values are K = 0.005 and 0.007, with n = 1.3 and 1.3, respectively. In comparison, Fromm also looked at the expected envelope for the family of all metallic elements cataloged and recommended values of K = 0.012 and n = 1.0; these values predict a shielding factor in Eq. 1 in the order of α = 1/420, as used in the Tox-tracker approach. There is significant scatter to the data and the precision of the predictions is seen to vary by up to an order of magnitude. Since these relationships must be validated post-test once the sample has returned to earth, this technique represents a post-processing analytical technique.

The purpose of this paper was to use CALPHAD computational thermodynamic modeling[7] to identify how chemical activity changes with temperature in the complex Ni-based superalloy family. The calculations were performed using the referenced Thermo-Calc database TCHEA4. This multicomponent database combines thermodynamic description and phase equilibria in high-entropy alloys (HEA); this database is also reliable for calculations on Ni-based systems. Similar to the TCNI databases,[8] it was assessed from the critical evaluation of many binary and ternary systems using the Parrot module of Thermo-Calc and enables predictions to be made over large temperature and compositional ranges. With these results we compared empirical near-real and analytical post processing evaporation tracking with the actual behavior of the sample. From these calculations, the TLV margin of safety for each elemental species was evaluated.

EXPERIMENTAL

Electromagnetic Levitation

Electromagnetic levitation allows processing of reactive molten metal alloy samples without the need for a container, thus simultaneously eliminating crucible-induced contamination and buoyancy-driven sedimentation. The ISS-EML facility, developed by Airbus Defense and Space, has the capability to run experiments in both vacuum and in inert gas environments. A high frequency alternating current generates a magnetic field which then induces a secondary field in a conductive sample; the sample is thus positioned by an approximately 150–170 kHz quadrupole field and independently heated by 350 kHz of dipole field supplied by the SUPOS (super-positioning) water-cooled coil. A one-color high-precision pyrometer measures the sample temperature with a $\pm$ 5 K error (resolution of $<$ 0.1 K above 873 K) with a frequency of 100 Hz and has an operating range of 1.45–1.80 μm. The Ni-based superalloys used for this project were run as a part of Batch 1 experiments by ThermoProp/ThermoLab for thermophysical property analysis. The samples were roughly of 6.5 mm in diameter, weighing 1 g. Twenty cycles of CMSX-10 and 25 cycles of MC2 were run in a 350-mbar inert Ar gas shielding atmosphere.

Alloy Selection

Two single crystal superalloys, CMSX-10 and MC2 were processed with argon gas shielding for this study. CMSX-10 is a third-generation superalloy developed by Canon Muskegon that has been used in commercial turbofan and industrial aeroturbine engines[9] while MC2 is a second-generation material developed by ONERA for single crystal military helicopter and jet turbine blade applications.[10] The composition and melting point of each alloy is listed in Table I.

RESULTS AND DISCUSSION

Activity Coefficient

The activity coefficients for the individual constituents of each alloy were calculated using the Thermo-Calc software TCHEA4 database. Results for the CMSX-10 alloy are displayed in solid, two-phase (solid + liquid), and superheated liquid regions plotted as a function of temperature in Fig. 2, with results referenced to the elements in their liquid state. Components are grouped to emphasize similar behavior. Ti, Ta, and Hf have extremely low activity coefficients, as do Mo, Nb, and Al. It would be expected that these constituents would not appreciably evaporate from solution over the expected temperature range. Ni and W have activity coefficients slightly below one; because the vapor pressure of W is extremely low, as seen in Fig. 1b, we would not anticipate significant evaporation for this species. The activity coefficient of Ni approaches ideal behavior and since the concentration and vapor pressure are significant it is prudent to track this behavior with care.

Co and Cr show significantly high activity coefficients at low temperatures, where evaporation is insignificant, and each of these elements decreases to approach a value slightly above one when superheated. The low vapor pressure of Re indicates that, like W, there will be limited loss of this constituent even though the activity coefficient is well above one. Co and Cr have high vapor pressures and high activity coefficients and these species need to be evaluated with care. For all species investigated, behavior just above the alloy melting point shows a linear trend and thus the activity coefficient values at the liquidus and at a superheat of 100 degrees are

Table I. Alloy nominal composition, melting point, and activity coefficient in solution

Material	Property	Cr	Co	Mo	W	Ta	Nb	Re	Al	Ti	Hf	Ni
CMSX-10	wt.%	2.0	3.0	0.4	5.0	8.0	0.1	6.0	5.7	0.2	0.03	~ 70
T_m = 1706 K	γ (T_m)	1.20	1.32	9.93×10^{-2}	5.91×10^{-1}	2.99×10^{-4}	2.76×10^{-2}	2.25	6.35×10^{-3}	1.45×10^{-3}	2.60×10^{-5}	7.99×10^{-1}
	γ (T_m + 100)	1.18	1.31	1.10×10^{-1}	6.39×10^{-1}	4.91×10^{-4}	4.46×10^{-2}	2.01	1.05×10^{-3}	3.02×10^{-3}	6.21×10^{-5}	8.11×10^{-1}
MC2	Wt. %	8.0	5.0	2.2	8.0	6.0	–	–	5.0	0.5	–	~ 65
T_m = 1661 K	γ (T_m)	1.27	1.20	7.91×10^{-1}	8.47×10^{-1}	3.85×10^{-4}			6.71×10^{-3}	2.00×10^{-3}		7.46×10^{-1}
	γ (T_m + 100)	1.22	1.20	8.72×10^{-1}	9.04×10^{-1}	6.51×10^{-4}			1.12×10^{-2}	3.97×10^{-3}		7.58×10^{-1}

also included in Table I for potential use in future Tox-tracker software upgrades.

Based on knowledge of the activity coefficients, the time–temperature profile for each cycle was applied using the analytical calculation approach. Unlike for the empirical technique, the output mass and composition from one cycle were used as inputs to the subsequent cycle. Typical results are shown in Fig. 3 where mass is displayed as a function of time in Fig. 3a. Note that the axis scale for mass loss was accentuated to highlight loss during this first melt cycle and within this cycle the total loss was only in the order of 5 μg. The loss of each constituent is tracked in Fig. 3b and shown as a part per million value to accentuate the influence of the elemental composition of each constituent in the alloy on a relative mass loss basis. The rate of mass loss is highest during the time that the sample is superheated. This is readily evident in Fig. 3c where the loss rate is plotted as a function of time; only Cr evaporates significantly on an absolute mass loss basis. As noted previously, Cr contributes significantly to the total mass loss, especially at high superheat values.

Table II contains a summary of the predictions using the two approaches and compares them with the observed mass loss during space testing; both approaches provide consistent estimates of overall loss. The empirical Tox-tracker prediction is higher than the analytical approach in all cases, meaning that since its primary purpose is astronaut safety it is justifiably conservative, and the agreement with the measured loss in both approaches is better for MC2 than for CMSX-10. Interestingly, since the activity coefficient of Ni, Co, and Cr approach $\gamma = 1$ in the superheated condition, use of the ideal solution model, as is done by the Tox-tracker, appears to be an appropriate simplification. The only caveat to this observation is that the low activity coefficient of aluminum is due to the strong attractive Al interactions and negative mixing enthalpy within the liquid phase, evaporation of this species should be significantly reduced from the ideal values. Furthermore, the previous approach [4] where the γ_{Al} was set to zero based on observed ESL vacuum evaporation testing, before activity coefficients were known, appears to be an appropriate simplification as well.

The precision of the predictions in Table II using the analytical approach are in the order of $\pm$ 0.03 mg and $\pm$ 0.01 mg, for CMSX-10 and MC2, respectively, based solely on errors associated with temperature measurement. Errors associated with the limitations inherent in the evaluation of element-specific fit parameters in Eq. 3 could introduce an error of up to an order of magnitude but using post-processing evaluations the transition metal fit parameters for Cr were set to mirror Ni such that $K = 0.005$ and $n = 1.4$, while Al was set to mirror the Fromm recommendation for the entire family of metallic elements as discussed previously. It would

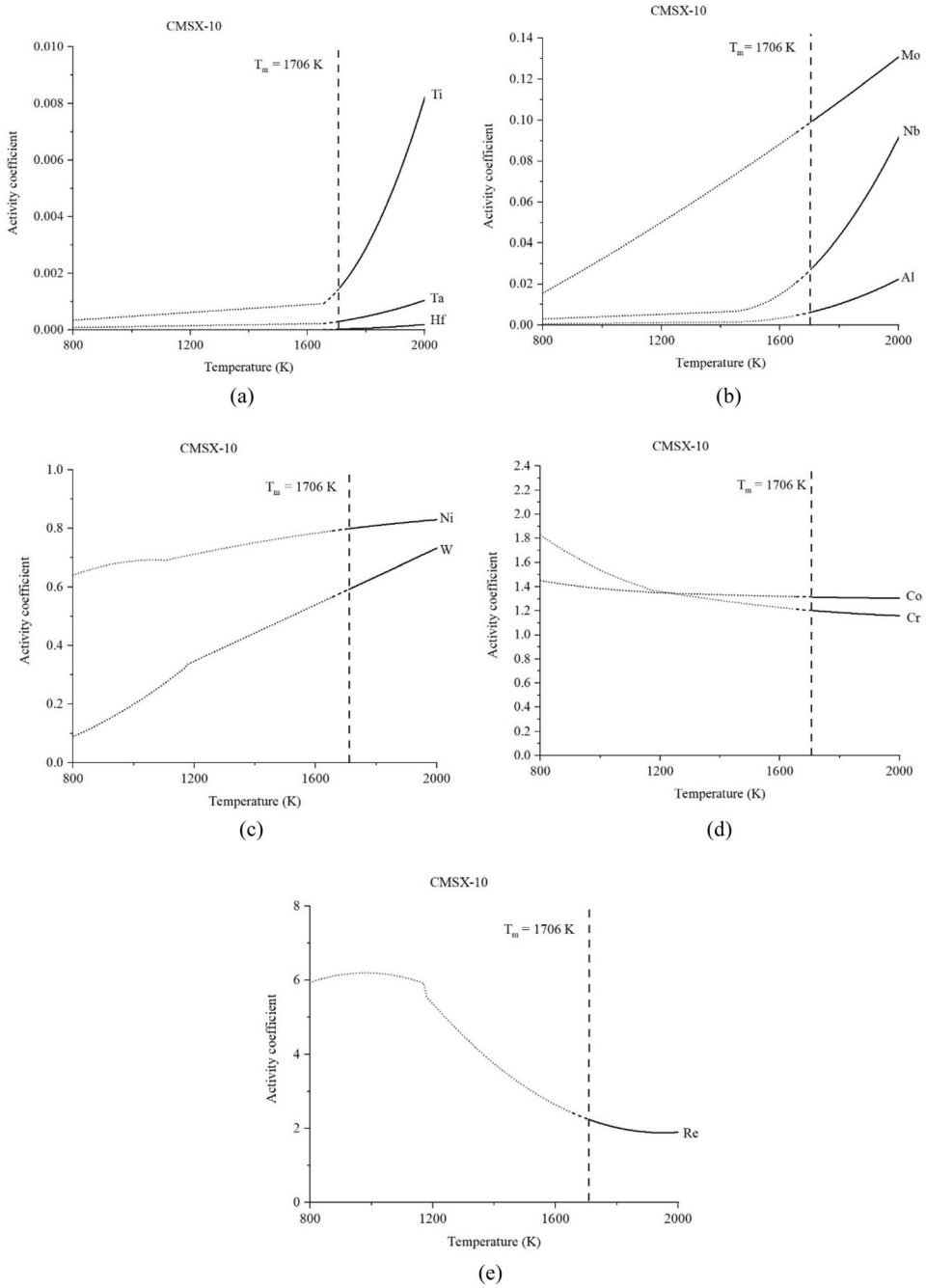

Fig. 2. Activity coefficients of CMSX-10 constituents, *light dash* solid, *heavy dash* two-phase, *bold* liquid. (a) Ti, Ta, Hf; (b) Mo, Nb, Al; (c) Ni, W; (d) Co, Cr; (e) Re

be of interest to attempt to validate the predictions of the potential for composition shift from preferential evaporation of volatile species, as was done by post-test elemental analyses for vacuum ESL testing,[4,5] but for space tests the argon gas shielding was particularly effective in reducing losses and the gross amount of material lost was insufficient to significantly shift the overall composition with regards to any component in solution.

Additional error is introduced through use of computational thermodynamics to attempt to quantify element-specific activity in solution. But, due to the numerous phase diagram data and thermodynamic quantities used to optimize a system, the quantification uncertainty associated with the

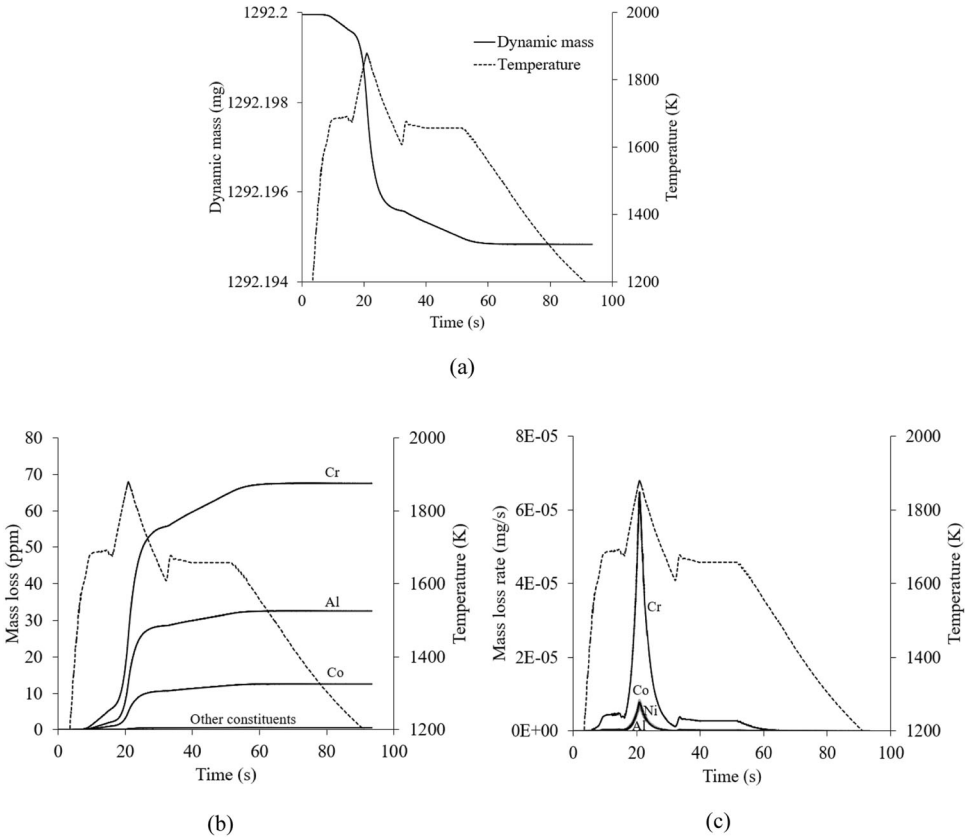

Fig. 3. Typical evaporation loss tracking results for the first of twenty CMSX-10 melt cycles. (a) Time–temperature-mass profile, (b) cumulative loss by species, and (c) species loss rate

Table II. Mass evaporation overview

Material	Pre-launch mass (mg)	Post mission mass (mg)	Observed loss (mg)	Empirical prediction (mg)	Analytical prediction (mg)
CMSX-10	1292.20	1291.96	0.24	0.70	0.42
MC2	1225.00	1224.75	0.25	0.23	0.20

Table III. Safety margin for Tox-tracker and activity coefficient corrected models

		CMSX-10 TLV margin		MC2 TLV margin	
Element	Limit (mg)*	Empirical approach	Analytical approach	Empirical approach	Analytical approach
Ni	96	2369	2368	9571	6145
Cr	32	627	234	584	488
Co	1.28	916	32	1838	84
Al	64	106	319	384	637

*Assumes an ISS cabin volume of 64 m^3

CALPHAD assessments is hard to establish. Even if the uncertainty estimation for computational thermodynamics is critically evaluated,[11,12,13] the reliability of the databases relies on comparisons with experimental phase equilibria or thermodynamic data of higher order systems and commercial alloys. Predictions can only be validated by experiment and, as noted above, anticipated shifts in composition from the current experiment are insufficient to provide this validation.

Since astronaut safety is a prime concern, the element-specific predictions from both approaches are compared with the TLV limit requirements. Table III displays the NASA imposed limit for each element that evaporates significantly for these superalloy compositions and the TLV margin, a safety factor calculated as the ratio of limit to prediction, for each of the predictive model approaches. Elements with a margin exceeding ten million (10^7) are not listed because the potential for astronaut health risks have been fully mitigated; the predicted evaporation was insignificant when compared to the limit and none of these elements pose a hazard.

All species fall well below the required toxicity hazard limit. By including the influence of activity coefficients using the analytical approach, the margins for all species except Al are decreased; this indicates that activity coefficient calculations are important to ensure astronaut health. The margin for both Ni and Cr are only slightly reduced, mainly because their activity coefficients were near one and thus ideal solution and non-ideal solution behavior is comparable. Co has the highest transition metal activity coefficient and the divergence is thus more pronounced, making it the most critical species to be tracked during superalloy processing. In comparison, with the significant reduction in activity coefficient for Al, the predicted evaporation of this species is significantly reduced and thus the margins increase when using the analytical approach. Future work is recommended to include the activity coefficient evaluation and element-specific inert gas shielding factors into the Tox-tracker protocols. Including the dynamic change to area based on density as a function of temperature and change in volume with loss of material are unwarranted due to the effectiveness of gas shielding in reducing the potential for dust generation.

CONCLUSION

The Langmuir computational approach provides excellent agreement with the observed behavior. This post-mission analytical predictions show only marginal improvement over the pragmatic near-real time Tox-tracker empirical approach. The differences are relatively insignificant for the nickel-based superalloys investigated, and the empirical approach is slightly more conservative, as would be desirable for an astronaut risk mitigation tool. Use of computational thermodynamic simulations increases confidence in establishing health safety margins for alloying elements in these alloys. Ni, Co, and Cr have activity coefficients near one and thus behave in a manner consistent with an ideal solution model. Al has an extremely low activity coefficient and evaporation is relatively small despite the large vapor pressure. Other elemental alloying elements have low activity coefficients and low vapor pressure and can be ignored for the superalloys. Argon shielding is particularly effective in decreasing the evaporative flux compared with testing in a vacuum, with improvements of around a couple of orders of magnitude. Both the empirical and analytical techniques provide corroboration that testing can be accomplished without changing the composition of the test material and, most importantly, prove that the astronauts are adequately protected from potential hazards from dust exposure.

ACKNOWLEDGEMENTS

The authors acknowledge collaborative support by team members from the Microgravity User Support Center (MUSC) through access to the ISS-EML facility which is a joint undertaking of the European Space Agency ESA and the German Aerospace Administration DLR. This project was sponsored by NASA under grants NNX17AH41G and 80NSSC19K0256. The author also acknowledges support from the European Space Agency (ESA) and the German Space Agency (DLR) administration as this work was conducted under the collaborative framework of ThermoLab AO-2009-1020.

REFERENCES

1. S. Schneider, *Private communication based on MUSC documents EML-PR-AST-015_01_EML_Dust Limit Calculation, EML-FZJ-GSF-01-Measurement of Gas Shielding Factors, EML-DGRD-10, -11, -23, and EML-ESA-RQ-003_i1_Batch 1 DRG, Deutsches Zentrum für Luft- und Raumfahrt (DLR)* (Germany: Köln, 2019).
2. I. Langmuir, *Phys. Rev.* 2, 229 (1913).
3. C.B. Alcock, V.P. Itkin, and M.K. Horrigan, *Can. Metal. Q.* 23, 309 (1984).
4. J. Nawer, X. Xiao, M.P. SanSoucie, and D.M. Matson, *High Temp- High Press* 49, 17 (2019).
5. J. Lee and D.M. Matson, *Int. J. Thermophys.* 35, 1697 (2014).
6. E. Fromm, *Metall. Trans. A* 9A, 1835 (1978).
7. H. Lukas, S.G. Fries, and B. Sundman, *Computational Thermodynamics: The Calphad Method* (Cambridge: Cambridge University Press, 2007).
8. J. Bratberg, H-H. Mao, L. Kjellqvist, A. Engström, P. K. Mason, and Q. Chen, *Superalloys 2012*: eds E. S. Huron, C. Reed, M. C. Hardy, M. J. Mills, R. E. Montero, P.D. Portella and J. Telesman (TMS,2 012), 21, 803(2012).
9. G. L. Erickson, *Superalloys 1996*, eds. R.D. Kissinger, D.J. Deye, D.L. Anton, A.D. Cetel, M.V. Nathal, T.M. Pollock, D.A Woodford, (Warrendale: Materials Research Society, 1996), 35(1996).
10. P. Caron and T. Khan, *Aerosp. Sci. Technol.* 3, 513 (1999).
11. D.V. Malakhov, *Calphad* 21, 391 (1997).
12. P. Honarmandi, T.C. Duong, S.F. Ghoreishi, D. Allaire, and R. Arroyave, *Acta Mater.* 164, 636 (2019).

13. T.C. Duong, R.E. Hackenberg, A. Landa, P. Honarmandi, A. Talapatra, H.M. Volz, A. Llobet, A.I. Smith, G. King, S. Bajaj, A. Ruban, L. Vitos, P.E.A. Turchi, and R. Arróyave, *Calphad* 55, 219 (2016).